

# Three dimensional Finite Element modeling of seismic soil–structure interaction in soft soil



Hooman Torabi\*, Mohammad T. Rayhani

Department of Civil and Environmental Engineering, Carleton University, Ottawa, Ontario, Canada

## ARTICLE INFO

### Article history:

Received 19 August 2013

Received in revised form 21 March 2014

Accepted 24 March 2014

### Keywords:

Soft soil

Elasto-plastic constitutive model

Soil–foundation–structure interaction

Stiffness ratio

Period elongation

Foundation rocking

## ABSTRACT

Earthquakes in regions underlain by soft clay have amply demonstrated the detrimental effects of soil–structure interaction (SSI) in such settings. This paper describes a new three dimensional Finite Element model utilizing linear elastic single degree of freedom (SDOF) structure and a nonlinear elasto-plastic constitutive model for soil behavior in order to capture the nonlinear foundation–soil coupled response under seismic loadings. Results from an experimental SSI centrifuge test were used to verify the reliability of the numerical model followed by parametric studies to evaluate performance of linear elastic structures underlain by soft saturated clay. The results of parametric study demonstrate that rigid slender (tall) structures are highly susceptible to the SSI effects including alteration of natural frequency, foundation rocking and excessive base shear demand. Structure–foundation stiffness and aspect ratios were found to be crucial parameters controlling coupled foundation–structure performance in flexible-base structures. Furthermore, frequency content of input motion, site response and structure must be taken into account to avoid occurrence of resonance problem.

© 2014 Elsevier Ltd. All rights reserved.

## 1. Introduction

The observed damage and subsequent processing of strong ground motion recordings obtained from soft soil deposits during the 1985 Mexico City and 1989 Loma Prieta earthquakes have revealed the significant importance of seismic site response and SSI on the response of affected structures [1]. These data and others from instrumented sites have been used to verify the analytical methods developed for soil–structure interaction (SSI) prediction, and to calibrate numerical methods and soil constitutive models as well. Observation of SSI during field tests and laboratory model tests is difficult, especially for settings with complex geometries. Because of this, robust numerical modeling methods can be useful in SSI identification for engineering design purposes.

SSI can be defined as the mutual effects that the vibrating structure, the foundation and the ground have on each other, causing alterations in the vibrational characteristics of each. Basically, two mechanisms dominate SSI: *Kinematic* and *Inertial interaction*. Earthquake ground motion causes soil displacement in what is known as free field motion. The kinematic interaction effect results from the inability of a stiff foundation in or on the soil to move in

the same way as the free field motion of the sediment. The main factors contributing to the kinematic interaction include the foundation embedment, the motion-producing wave inclination and incoherency.

The kinematic interaction effect is usually quantified by a frequency dependent transfer function. This is defined as the ratio of the foundation motion (FIM) to the free field ground motion assuming a massless foundation and structure [2]. Veletsos et al. [2] improved the expression introduced by Luco and Wong [3] and derived a transfer function for a rigid massless rectangular foundation resting on viscoelastic half-space for both the translational and rotational (rocking) components of the foundation motion. The transfer function was obtained in terms of normalized incoherency parameters using a space invariant power spectral density function (PSD) for translational and cross power spectra for rotational motion assuming unidirectional free field ground motion.

Inertial interactions also affect the vibrational characteristics of structures. The inertial force of the vibrating structure produces base shear and moment effects at the foundation level resulting in relative displacement between the foundation and the soil. More importantly, inertial interactions also result in changes in the modal characteristics of the structure including variations in modal frequencies and damping factors. A simplified model has generally been used to investigate the inertial interaction phenomenon in

\* Corresponding author. Tel.: +1 (613) 292 7661.

E-mail addresses: [hooman\\_torabi@carleton.ca](mailto:hooman_torabi@carleton.ca) (H. Torabi), [mohammad.rayhani@carleton.ca](mailto:mohammad.rayhani@carleton.ca) (M.T. Rayhani).

theoretical and analytical studies [4–8]. This single degree of freedom system consists of frequency dependent translational and rotational springs, representing dynamic stiffness and damping of a flexible foundation–soil system.

Utilizing field test data in conjunction with SSI-identification analytical procedures has provided valuable insights into soil–foundation interaction in terms of impedance functions [9,10], kinematic interaction of soil–foundation based on calibrated models [11] and structure–foundation–soil interaction using the system identification method [12,13]. Moreover, several numerical investigations of SSI phenomena have been carried out taking into account nonlinear soil behavior and employing frequency domain Finite Element [14] and time domain finite difference methods [15].

The purpose of the current study is to develop a 3-D dynamic Finite Element (FE) simulation to capture seismic site response and coupled soil–foundation–structure interaction by taking into account the progressive softening (inelasticity) of soft saturated clay. This was accomplished by implementing an elasto-plastic constitutive model of soil to capture the elasto-plastic foundation–soil coupled response under irregular seismic loadings. Initially, model calibration using centrifuge tests conducted by Rayhani and Elnaggar [16] was carried out, followed by a parametric investigation of SSI. The analytical methods developed for SSI evaluation were used in the parametric study phase to investigate the capability of the soil-structure continuum model in predicting SSI effects. In this study, analyses were performed for linear elastic structures, represented by a single degree of freedom system (SDOF), supported by elastic foundation. The soil profile underlying foundation was assumed to be uniform with constant shear wave velocity to eliminate the effect of soil non-uniformity on SSI.

## 2. Soil–foundation–structure interaction

Generally, two concepts of “fixed-base” and “flexible-base” building are taken into account in any SSI evaluation process. The latter refers to a building founded on a soil deposit which enables the foundation of the building to vibrate when subjected to dynamic loadings. These conditions alter the vibrational characteristics of a fixed-base foundation compared to buildings founded on a rigid base. Several experimental studies using field test data and recorded strong ground motions and analytical analyses have been conducted on the effects of SSI on the modal response of structures. Two procedures have been recommended for the extraction of modal parameters for flexible-base and fixed-base buildings [12,17]. These approaches, known as “System Identification” methods, are used when recordings of the structure’s roof and foundation motions are available whereas free field ground motion as soil–foundation–structure input is missing. However, in the present study, all the input and output recordings for SSI evaluation are obtained.

Soil–foundation–structure interaction (SFSI) introduces complexities requiring thorough investigation of the contributing parameters. Veletsos and Meek [5] defined several critical parameters controlling the vibrational properties of fixed and flexible-base buildings by assuming a SDOF system resting on a viscoelastic half space soil (Fig. 4a). These dimensionless parameters are expressed in terms of the underlying soil shear wave velocity  $V_s$ , soil mass density  $\rho$ , structural mass  $m_s$ , effective height of the structure  $h_{eff}$ , fixed-base period of the structure  $T_s$ , and rotational  $r_o$  and translational  $r_u$  radius of an equivalent circular foundation, and are as follows:

$$\sigma = \frac{V_s T_s}{h_{eff}} \quad (1)$$

$$\gamma = \frac{m_s}{\rho \pi r_u^2 h_{eff}} \quad (2)$$

$$A = \frac{h_{eff}}{r_u} \quad (3)$$

The above defined parameters are the soil to structure stiffness ratio  $\sigma$ , structure to soil mass ratio  $\gamma$  and the aspect ratio  $A$ . When comparing the performance of flexible and fixed-base structures, changes in the modal vibrational parameters are important due to their direct consequences on base shear and foundation motion. Previous studies indicate that in the case of a flexible-base structure, oscillation occurs with a longer natural period ( $\bar{T}_s$ ) rather than the fixed-base natural period ( $T_s$ ), and the damping ratio ( $\bar{\zeta}$ ) increases compared to the fixed-base ratio ( $\zeta$ ). Base shear and FIM are influenced as a result [4,5,17]. Also, simplified analytical procedures confirm the significant roles of the structure to foundation stiffness ratio and the aspect ratio in period lengthening, and the associated impacts on structural demands [5,6].

Assuming the structure–foundation system to be a 2 DOF system (Fig. 4a) subjected to free field ground motion, the structure and foundation motion can influence the vibrational motions of each. An analytical solution is presented for the coupled equation of motion for this system for which two natural frequencies are obtained. Previous studies have shown that the structure to foundation stiffness ratio is a main contributing factor in structure–foundation interaction in flexible-base structures [5,12,18].

Safak [12] performed parametric analyses based on analytical solutions of coupled equations of motion for 2DOF system (Fig. 4a) assuming that the foundation rocking motion is negligible. It was shown that the fixed-base circular frequency ratio ( $\mu = \omega_s/\omega_f$ ) for the structure and foundation and their mass ratio ( $\eta = m_s/m_f$ ) affect the deviation in the natural frequency of the coupled system compared to the fixed-base system (period lengthening). The structure–foundation stiffness ratio can be expressed in terms of these parameters using equations of natural circular frequencies;  $k_s = m_s \cdot \omega_s^2$  and  $k_f = m_f \cdot \omega_f^2$  as follows:

$$r_k = \frac{k_s}{k_f} = \frac{m_s \cdot \omega_s^2}{m_f \cdot \omega_f^2} = \eta \mu^2 \quad (4)$$

where  $k_s$  and  $k_f$  are the stiffness of the structure and foundation, respectively. In addition to Eq. (4), the impedance function of the foundation ( $\bar{K}$ ) is a complex valued function controlling the force–displacement relationship between the foundation and the surrounding soil. This function consists of dynamic stiffness as the real part and the frequency dependent imaginary part as damping [8]:

$$\bar{K} = k_f + i\omega c \quad (5)$$

In Eq. (5),  $c$  is the damping coefficient including both radiation damping between the soil and the foundation and the hysteretic damping of the soil as well. The real part,  $k_f$  is the frequency dependent translational stiffness or the real part of the impedance function of a circular foundation resting on viscoelastic soil half space. It is expressed by Veletsos and Meek [5] as follows:

$$k_f = \alpha_u k_u \quad (6)$$

$$k_u = \frac{8}{2-\nu} G r_u \quad (7)$$

where  $\alpha_u$  and  $k_u$  are the frequency dependency coefficient accounting for embedment effect and the foundation static stiffness respectively.  $\nu$  and  $G$  are the Poisson ratio and the shear modulus of the underlying soil. Substituting the equation  $\omega_s = 2\pi/T_s$  and Eqs. 6 and 7 in Eq. (4) the relative stiffness is reformulated as follows:

$$r_k = \frac{m_s (2\pi/T_s)^2}{\alpha_u (8G r_u / (2-\nu))} \quad (8)$$

Employing classic shear modulus equation ( $G = \rho v_s^2$ ) and rearranging parameters in Eq. (8), the stiffness ratio equation can be expressed as:

$$r_k = \frac{\pi^3(2-\nu)}{2\alpha_u} \frac{(m_s/\rho\pi r_u^2 h_{eff})}{(V_s T/h_{eff})^2} \frac{1}{(h_{eff}/r_u)} \quad (9)$$

The crucial dimensionless parameters for SSI characterization appeared in the above equation can be simplified as following by substituting Eqs. (1)–(3) in Eq. (9):

$$r_k = \frac{k_s}{k_f} = \frac{\pi^3(2-\nu)}{2\alpha_u} \frac{\gamma}{\sigma^2 A} \quad (10)$$

Eq. (8) has previously been presented by Zhang [18] and is similar to the relative structure to foundation stiffness parameter ( $\theta$ ) proposed by Bielak [4]. It is expressed as a function of the aspect ratio ( $A$ ) and the soil to structure stiffness ratio ( $\sigma$ ) which are believed to be crucial variables.

### 3. 3D Finite Element model

The open source framework for earthquake engineering simulation “OpenSees”, (Open System for Earthquake Engineering Simulation), [19] was utilized to develop a numerical model and investigate seismic site response and soil–foundation–structure interaction in soft soils. The FE based OpenSees framework includes advanced structural and geotechnical models enhancing earthquake engineering simulations.

#### 3.1. Constitutive model

The multi-yield-surface J2 plasticity (Von Mises) model was employed to simulate the non-linear shear behavior of saturated soft clay underlying the foundation (Fig. 1). The plasticity model is based on a purely deviatoric kinematic hardening rule with associative flow rules [20]. The volumetric stress–strain behavior is linear elastic, and plastic response is induced by deviatoric shear stress. Thus, the translation of the yield surface is allowed in deviatoric stress space and the hysteretic shear response of the soil is well captured as a result. In this model, the hyperbolic curve represents the hysteretic cyclic shear stress–strain response of the soil (back bone curve). This model was finally improved and implemented in OpenSees by Elgamal et al. [21] as pressure independent multi-yield material. It is an effective model to simulate the undrained cyclic response of saturated cohesive soils and soil–structure interactions under both cyclic and earthquake loadings. According to this model, 9 input parameters are essential to define cohesive soil stress–strain response. All of these parameters are

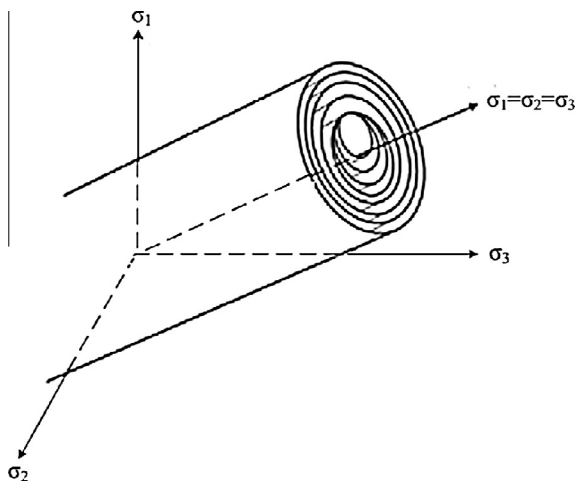


Fig. 1. Kinematic hardening elasto-plastic constitutive model with Von-Mises multi-yield surfaces [modified from [22]].

simple, basic terms used to describe the mechanical behavior of any soil.

#### 3.2. Development of soil–structure model

In this study, the soil domain was modeled by employing 3D 8-node Brick elements. Each node has three translational degrees of freedom. The pressure independent multi-yield material was assigned to the soil element to simulate the nonlinear cyclic behavior of saturated soft clay. Two different types of structures were modeled. In the model verification step, the elastic 8-node Brick elements represented the model structure and its embedded shallow foundation. In the second step, in order to model a simplified SDOF system with specified modal frequency and damping, a 3D linear elastic beam–column element was selected to represent the stiffness and height of the model structure, and a lump mass to represent the structure’s mass. The nodes connecting this type of element have six degrees of freedom of which three are for translation and three are for rotation. All the model materials assigned to structural elements are linear isotropic elastic material. Further details on the material properties are described in the following sections of this paper.

#### 3.3. Governing equation and numerical solution

The seismic response of the soft clay deposit and structure is estimated by time domain numerical solution of the soil–structure dynamic equilibrium equation defined as [23]:

$$[M]\{\ddot{u}\} + [C]\{\dot{u}\} + [K]\{u\} = -[M]\{\ddot{u}_g\} \quad (11)$$

where  $[M]$ ,  $[C]$  and  $[K]$  are the mass, viscous damping and stiffness matrix of the soil–structure system, respectively. The  $\{u\}$  matrix denotes the relative nodal displacement matrix, and  $\{\ddot{u}_g\}$  is the nodal acceleration imposed at the base of the model. The viscous damping matrix  $[C]$  of the system is calculated using the proportional Rayleigh damping method which is described in the following sections of the paper. The stiffness matrix is calculated at each time-step using the constitutive model formulation describing cyclic and static stress–strain behavior of the soil and structure materials. Each analysis consists of static and dynamic loading steps; in the first step, soil and structure are allowed to undergo deflection under gravitational static loadings, then the input motion is applied at the base of the model. The time domain numerical integration was carried out using the Newmark algorithm method with parameters of  $\alpha = 0.6$  and  $\beta = 0.3025$  to eliminate noisy frequencies that are developed by standard Newmark parameters ( $\alpha = 0.5$ ,  $\beta = 0.25$ ) [24].

## 4. Model verification

#### 4.1. Centrifuge tests

Physical modeling of geotechnical events has been widely performed in recent decades. Such densely instrumented 1-g shaking table and centrifuge tests provide reliable benchmarks and datasets for numerical simulation tools [25]. The centrifuge model test conducted on the C-CORE centrifuge located at Memorial University in Newfoundland, Canada, has been selected as the target test for the verification of numerical modeling [16]. In this experiment, the test model was spun in a centrifuge at a radial acceleration of 80 g. A rigid hollow aluminum box with dimensions of 5.5 m in length, 2.5 m in width and 6 m in height in prototype scale was placed on top of a synthesized soft clay material called Glyben. The schematic configuration of the centrifuge model is shown in Fig. 2. This box was embedded 2 m deep in the soil, representing

a shallow foundation. A rigid walled soil container with dimensions of 0.73 m length, 0.3 m width and 0.57 m height was used to contain the soil-structure model, simulating a uniform 30 m deep soil layer in the prototype scale. The artificial clay “Glyben” is a mixture of glycerine and bentonite with a mixing ratio of 45% and 55%, respectively. The void ratio of tamped Glyben within the container was 2.11 resulting in a bulk density of 1.575 kg/m<sup>3</sup>. The T-bar and cyclic triaxial test results indicate an ultimate undrained shear strength of 50 kPa obtained at a maximum shear strain of 10%. Also, results of laboratory dynamic element tests such as resonant column and cyclic triaxial suggest the shear modulus ( $G$ ) to be 8000 kPa at a confining pressure of 100 kPa. However, thixotropy and pre-test consolidation effects in increasing the shear modulus must be taken into account when implementing “ $G$ ” as an input parameter into the model [26,27].

#### 4.2. Parameter definition

The soil profile consists of uniform 30 m deep soft clay (Glyben) with the mechanical properties illustrated in Table 1. These parameters were used as input data for the J2 plasticity (Von Mises) constitutive model. As shown in Table 1, zero was set as the undrained friction angle of the soil, because it is assumed that the cyclic shear behavior of the clay is independent of the confining pressure due to the negligible pore pressure dissipation and the rapid rate of earthquake loadings, thus only the soil skeleton is involved in shear wave propagation [28].

##### 4.2.1. Rayleigh damping

Generally, the stress–strain behavior of cohesive soils is highly dependent on the strain rate, and exhibits a viscous response. Also, the damping ratio of Glyben was observed to be 10–15% higher than that of most previously tested clays [26]. This can be attributed to the presence of highly viscous Glycerin as the pore fluid. Thus, in addition to hysteretic damping generated by the elastoplastic soil model, Rayleigh damping was implemented in the model to not only account for additional damping of Glyben but also to reproduce small strain frequency independent damping associated with geomaterials in the frequency range of interest [29]. According to the Rayleigh damping formulation, two coefficients  $a_0$  and  $a_1$  are applied to the mass and stiffness matrices of the system, respectively, and are determined by Eqs. (13) and (14) using two frequencies  $f_1$  and  $f_2$  and their corresponding damping ratio  $\zeta_{1,2}$ . However, in such a frequency range damping ratio becomes slightly lower than the specified one ( $\zeta_n$ ) and reaches minimum value  $\zeta_{min} = \sqrt{a_0 a_1}$  at  $\omega_{min} = \sqrt{a_0/a_1}$ .

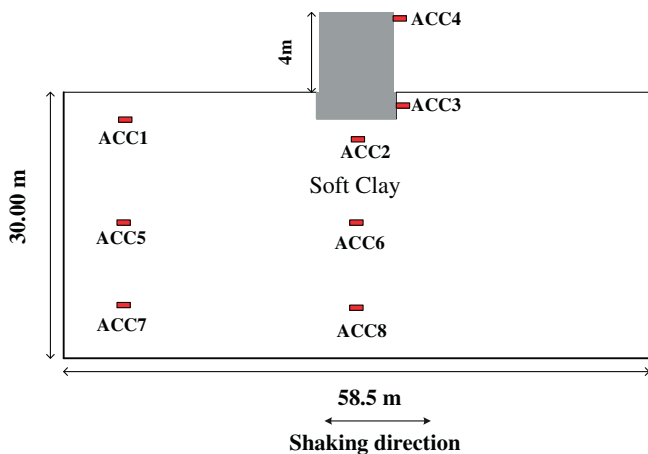


Fig. 2. Side view of SSI centrifuge test [16].

**Table 1**  
Material parameters for soft clay.

Model soil parameters	Parameter index	Value
Bulk mass density (kg/m <sup>3</sup> )	$\rho$	1575
Shear modulus (kPa)	$G_{max}$	9600
Bulk modulus (kPa)	$B$	65,380
Undrained shear strength (kPa)	$S_u$	50
Undrained friction angle	$\phi_u$	0
Poisson ratio	$\nu$	0.43
Reference confining pressure (kPa)	$P_r$	100
Peak shear strain	$\gamma_{max}$	0.1

$$C = a_0 M + a_1 K \quad (12)$$

$$a_0 = \frac{2\zeta\omega_1\omega_2}{\omega_1 + \omega_2} \quad (13)$$

$$a_1 = \frac{2\zeta}{\omega_1 + \omega_2} \quad (14)$$

where  $\zeta = \zeta_1 = \zeta_2$  and  $\omega = 2\pi f$  is the circular frequency in rad/s. Based on experimental response spectra, the effective frequency range of system was specified by boundary frequencies of  $f_1 = 0.5$  and  $f_2 = 5$  Hz for model verification. This range encompasses natural frequencies of site and structure and predominant frequency of input motion as well. Using Eqs. (13) and (14) and employing  $\omega_1$ ,  $\omega_2$  and  $\zeta_{1,2} = 12\%$ , the mass and stiffness coefficients were obtained as 0.685 and 0.007, respectively, resulting in  $\zeta_{min} = 7\%$  at  $f_{min} = 1.6$  Hz. Assigning Rayleigh damping as described ensures that major frequencies of system are not subjected to over-damping, and damping with slight deviation from desired value dominates in effective frequency range of the system. It should be noted that unlike the verification stage, in parametric study phase, a frequency range of 0.1 to 10 Hz was set as effective range and 2% Rayleigh damping was assigned to the soil to account for small strain damping of natural soils.

#### 4.3. Mesh generation and boundary conditions

In current numerical model, the soil medium was discretized into 13304 8-node Brick elements with 15360 surrounding nodes. The structure was modeled in the shape of a hollow box to simulate the structure configuration used in the centrifuge test. It was made up of elastic isotropic material assigned to 272 8-node Brick elements, and 190 equal degrees of freedom (equalDOF) constraints were used to connect structural nodes to soil nodes at soil-structure boundaries. The mechanical characteristics of the rigid structure are described in Table 2.

To satisfy the rigid boundary conditions in the centrifuge test, soil nodes located at lateral and longitudinal side boundaries were fixed against translation in three directions. However, the shear-beam type lateral boundary condition in the direction of input excitation is highly recommended in numerical modeling of geotechnical events in order to comply with free field conditions and the deformable elastic lateral boundary conditions existing in the field [25]. Moreover, to avoid large numerical and time efforts, the model was reduced to half size due to symmetry of the model along the shaking direction in such a way that all the nodes on the

**Table 2**  
Material parameters for model aluminum hollow box.

Parameters	Parameter index	Value
Bulk mass density (kg/m <sup>3</sup> )	$\rho$	2800
Elasticity modulus (kPa)	$E$	$7 \times 10^7$
Poisson ratio	$\nu$	0.35

symmetry surface were restrained against displacement in the y-direction.

4.4. Verification of results

Representative simulation results including response spectra (5% damping) and time histories of the computed and recorded accelerations at various locations in the model are presented in Fig. 3. These locations include the free field (ACC1), underneath the structure (ACC2), the foundation (ACC3) at depths of 3.5 m, 4 m and 1 m respectively and the top of the structure (ACC4). Satisfactory agreement was observed between recorded and computed accelerations over both the time and frequency ranges at all locations except for ACC1. As observed in the acceleration response spectra (ARS) corresponding to ACC1, some spectral ordinates corresponding to a narrow frequency range of about 2–5 Hz were not reproduced by the numerical model accurately. Almost the same discrepancy was observed for the other accelerometers (ACC5 and ACC7) located at deeper levels of free field. Considering that ACC1 represents free field motion, such a discrepancy can be mainly due to numerical limitations in modeling the rigid boundary condition where some frequencies are amplified. In general, comparison of experimental and numerical results demonstrates the capability of the elasto-plastic soil constitutive model in simulating a dynamic SSI problem.

5. Parametric study

Any seismic soil–structure event involves three general aspects of free field ground motion, kinematic and inertial interactions; each with a significant role in the prediction of structure and foundation responses under soil–foundation–structure interaction (SFSI). Therefore, any seismic analysis must account for the contribution of each aspect in the SFSI event individually. In this study, the parametric investigation aims to develop an idealized continuum Finite Element model of SFSI using a SDOF system overlying a nonlinear soil deposit to assess various aspects of this event as well as the applicability of continuum models in the simulation

of SFSI. Fig. 4 schematically illustrates the present FE model (4b) and simplified SFSI model (4a) used by many studies excluding foundation mass [5,13] and those accounting for foundation mass [12,18]. For these SDOF or 2DOF systems, stiffness and damping coefficients for spring and dashpot elements are defined using analytical procedures [5,8], and recorded free field ground motion is applied at the free end of the spring and dashpot. Contrarily, the continuum nonlinear FE model not only simulates free field and SFSI response as a unique system but also introduces strain induced (hysteretic) damping to the soil–foundation interaction.

Fig. 5 demonstrates a schematic view of the discretized large model developed using OpenSees with a soil domain and a real building for better visualization. The generated model was visualized using GiD software [30]. The soil domain is 132 m long, 60 m wide and 30 m deep with boundaries far enough from the foundation to minimize the boundary effects. As mentioned earlier, the SDOF system represents a viscous linearly elastic structure with identified natural period and damping. Five percent viscous damping was assigned to the mass and stiffness matrix of the model structure (beam-column elements) using the Rayleigh damping formulation. The dynamic response of the structure was assumed to be dominated by first mode oscillation. Thus, to obtain such a response, two thirds of the structural mass was lumped at two thirds of the structure height (effective height) [14]. Four types of typical urban structures resting on shallow foundations were the main target structures to be modeled in this study. Table 3 summarizes the properties of the structures used in numerical models, which includes number of stories, aspect ratio, mass of structure, range of fixed-base natural periods and corresponding relative stiffness ratios. The fixed-base damping ratio assigned to the structure was selected to be 5%. The length, width and mass of elastic foundation used throughout the analyses are 12 m, 10 m and 288 tons, respectively. For the combined kinematic and inertial interaction analyses, the foundation was embedded 1.5 m in soil deposit, however, for the purpose of kinematic interaction, foundations of the same size were used with varying depth ratios ( $e/r$ ). Also, to mimic 1D shear wave propagation, the shear-beam type boundary condition was implemented by forcing the boundary nodes at the same elevation to undergo equal longitudinal and vertical displacement.

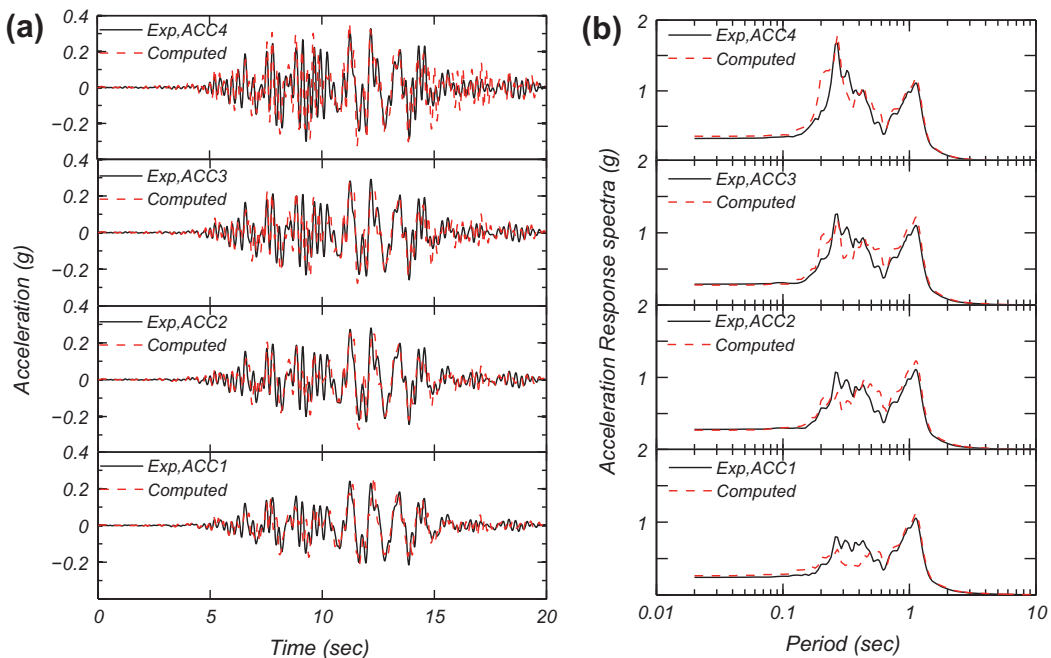


Fig. 3. Comparison of computed results with the SSI centrifuge test [16]. (a) Acceleration time histories and (b) acceleration response spectra.

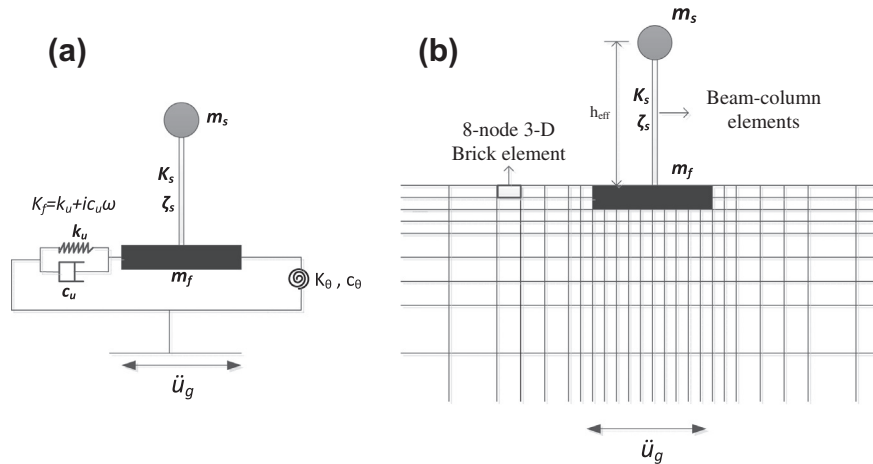


Fig. 4. (a) Simplified SFSI model. (b) Finite Element method used in this study.

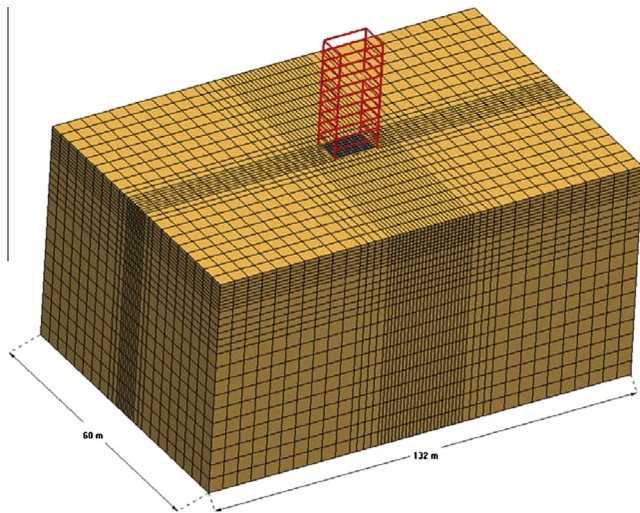


Fig. 5. Three dimensional view of Finite Element mesh.

The 1989 Loma Prieta earthquake (PGA = 0.4 g) recorded at station Gilroy No. 1 (outcrop motion) and the 1994 Northridge earthquake (PGA = 0.25 g) recorded at station Century City (which are available at [http://peer.berkeley.edu/peer\\_ground\\_motion\\_database](http://peer.berkeley.edu/peer_ground_motion_database)) were employed as input base excitations to investigate the effect of the frequency content of the input motion on SSI. The acceleration time histories and power spectra of these two input motions are shown in Fig. 6. Comparing the power spectra of the two ground motions, the Northridge earthquake includes low frequency components with higher amplitudes than the Loma Prieta earthquake. These long period (low frequency) spectra are believed to produce large displacements resulting in further softening of soft soils. This will be shown by the site response spectra in the following sections of this paper.

Table 3  
The properties of structure used in SSI numerical models.

Story	Aspect ratio ( $h/r$ )	Stiffness ratio ( $r_k$ )	Building mass ( $m$ ) (tons)	$T_n$ (s)
4	1.4	0.094–0.59	436	0.2–0.5
6	2	0.058–0.93	653	0.2–0.8
8	2.7	0.06–0.31	871	0.4–0.9
10	3.4	0.23–0.69	1089	0.5–1.2

## 6. Results and discussion

All the foundation-structure models overlaying 30 m of uniform soft clay were subjected to the two input motions from actual recorded earthquakes. The obtained results are discussed in three main categories including seismic site response, kinematic and inertial soil–structure interactions.

### 6.1. Estimation of transfer functions for SFSI

The transfer function, or frequency response function, is a mathematical tool for the identification of a system with deterministic input  $x(t)$  and output  $y(t)$  signals. In the context of seismic analyses, the ratio of the Fourier spectrum amplitudes of input and output signals represents the transfer function; however, this ratio is usually associated with spiky components due to the very small (near zero) amplitude of the denominator as a result of noise presence and signal randomness. Accordingly, transmissibility functions  $H(i\omega)$  were used to estimate transfer functions for both site response and kinematic and inertial structure–foundation-free field interactions. Transmissibility functions are formulated based on auto power spectra ( $S_{xx}, S_{yy}$ ) and cross power spectral density function ( $S_{xy}$ ) of input and output signals as follows [31]:

$$H_1(i\omega) = \frac{S_{xy}}{S_{xx}} \tag{15}$$

$$H_2(i\omega) = \frac{S_{yy}}{S_{xy}} \tag{16}$$

### 6.2. Free field site response

The evidence of severe damage and recorded strong ground motions in soft soil deposits during the 1989 Loma Prieta and 1985 Mexico City earthquakes demonstrated the capability of this type of soil to amplify the bedrock motion [1,32]. Subsequent

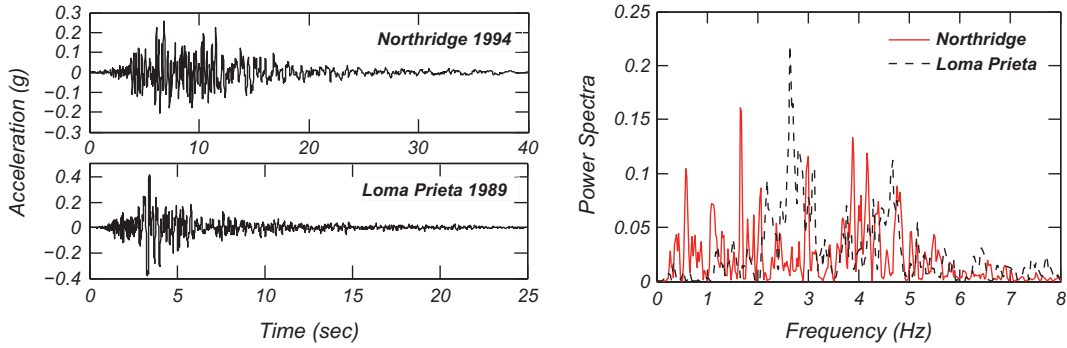


Fig. 6. Acceleration time histories and power spectra of Northridge 1994 and Loma Prieta 1989 earthquakes.

investigation into this phenomenon led to the development of site categories which were implemented in the building design code provisions (NEHRP 1997, NBCC 2010). According to this classification, which is based on average shear wave velocity in the top 30 m ( $v_{s,30}$ ), soft soil deposits with  $v_{s,30}$  less than 180 m/s are classified as group E. In this study, site specific analysis is conducted on a 30 m soil deposit with shear wave velocity of 78 m/s (site class E). The site response spectra and site amplification factor, which is the ratio of the response spectra of the free field and base motion in the frequency domain, are shown in Fig. 7.

As shown, three local peaks in the amplification function mark the fundamental modes of soil deposit vibrations. The first fundamental site period at which the greatest amplification occurs is at 2.15 s which is almost 30% greater than the elastic fundamental period obtained from the analytically derived equation  $T_g = 4H/v_s$  for damped vibration of soil deposited on rigid bedrock [33]. Furthermore, fairly large amplification is observed over a broad range of long periods ( $T_g > 1$ ). Such a period shift can be attributed to the soil softening and shear modulus reduction as the shear waves propagate through the soil deposit. Also, comparing the amplification factors of two different input motions, the

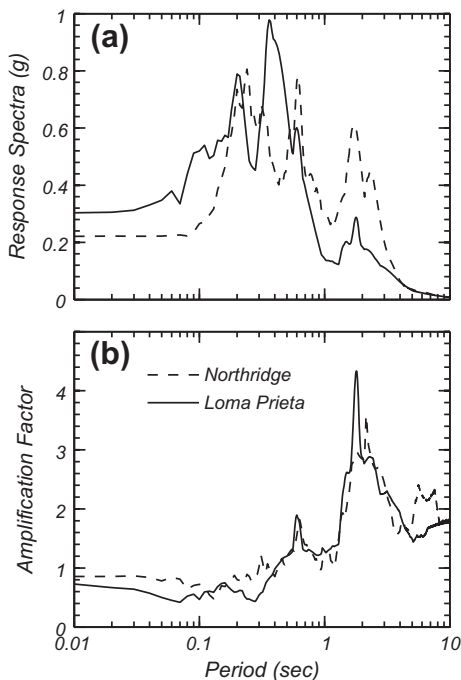


Fig. 7. (a) Acceleration response spectra for the free field motion (b) free field amplification factor.

first natural period of the Northridge earthquake demonstrates a larger shift caused by further softening of the soil deposit, which is a consequence of subjecting the soil to a higher number of low frequency cycles.

### 6.3. Kinematic interaction

When an embedded rigid shallow foundation is subjected to a strong ground motion, kinematic interaction causes the foundation motion to deviate from that in the free field. Accordingly, a reduction in amplitude of the foundation translational motion occurs, while foundation rocking motion is introduced as a result [8,34,35]. Several analyses with massless foundations and structures were carried out to evaluate the effect of foundation embedment on foundation motion due to the kinematic interaction mechanism. The rectangular foundation dimensions are 10 m in width and 12 m in length. Two types of massless foundation, including rigid core mat foundation and mat with basement wall foundation for shallow and relatively deep embedment, respectively, with equivalent circular foundation radii ( $r = 6.2\text{m}$ ) were employed in numerical analyses. The ( $e/r$ ) ratio denotes the embedment ratio which is the only variable in these analyses since wave propagation in this study is completely coherent and vertical. Investigation of incoherent or inclined incident waves is not the purpose of this study. The results of kinematic interaction effects on the horizontal foundation motion for different embedment ratios are illustrated in Fig. 8a. The horizontal foundation motion deviation is expressed in terms of the transmissibility function, defined in Section 4.1.2, denoted by  $\sqrt{S_{ff}/S_{gg}}$  in normalized frequency domain ( $\omega r/v_s$ ), where  $S_{ff}$  and  $S_{gg}$  are auto power spectra functions of translational foundation and free field ground motions, and  $\omega$ ,  $r$  and  $V_s$  are circular frequency, equivalent radius and shear wave velocity of soil, respectively [2,34].

As illustrated in Fig. 8a, foundation translational motion decreases up to 50% for the greatest embedment ratio ( $e/r = 0.65$ ) as the frequency increases, and embedment ratio significantly affect the level of deviation of foundation motion from that of free field. This effect is attributed to the distinct difference in the foundation and surrounding soil rigidity, resulting in frequency dependent radiation damping and energy dissipation as seismic waves spreading away from vibrating foundation to the soil medium [8,34,35].

In order to validate the kinematic interaction results, Fig. 8b compares transfer function estimated by current elasto-plastic FE model with that of analytical based method proposed by Elsabee and Morray[34] for foundation embedded in visco-elastic half space. The comparisons are performed for the embedment ratios of 0.25 and 0.48, which are shown by thin and thickened outlines, respectively in Fig. 8b. As shown, consistent trend is observed between two methods for both embedment ratios within effective

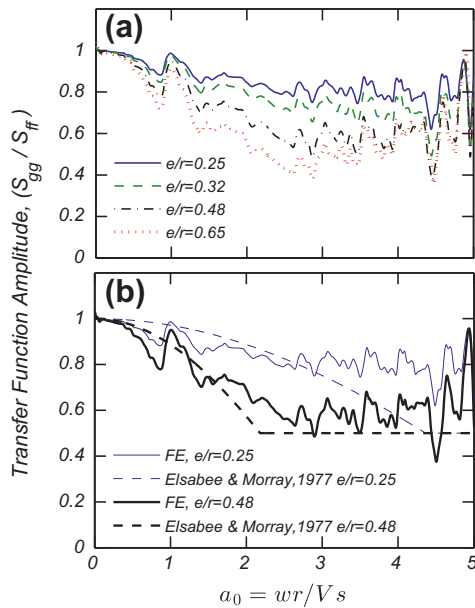


**Fig. 8.** (a) Kinematic interaction effect by massless foundation/free field transfer function for various depth ratios in normalized frequency domain (b) comparison of current elasto-plastic FE model with the visco-elastic analytical method by Elsabee and Morray [34].

frequency range of system ( $a_0 < 3$ ), above which satisfactory agreement can still be observed for deeper foundation. In high frequency range where radiation damping dominates, elasto-plastic FE model estimates lower deviation of foundation motion than analytical. Such lower prediction can be attributed to the soil plasticity that can influence radiation damping of foundation motion [36]. In summary, results of the kinematic interaction analysis shown in Fig. 8a demonstrate that this phenomenon can be beneficial to the reduction in foundation input motion.

#### 6.4. Inertial interaction

A set of analyses including 28 shaking events was performed to identify the contributions of the aspect ratio, the structure-foundation stiffness ratio and the frequency content of the input motion on SFSI, and the associated effects on structural demand. As summarized in Table 3, four main buildings with specified rectangular foundation size as in Section 5 and the embedment ratio of 0.25 were utilized as the structural model in all events. The mass ratio ( $\gamma = 0.16$ ), which is recommended for conventional buildings [37], was kept constant in all events. To illustrate the period lengthening, the flexible-base frequency was obtained from the transmissibility functions defined in Section 6.1, and computed using the acceleration recordings of the roof and free field. The roof/free field pair was considered as the input and output motions for the flexible system [10,12,13].

##### 6.4.1. Effect of stiffness ratio on period elongation

To illustrate the stiffness and aspect ratios influence on period elongation, Fig. 9 plots the data points obtained from the shaking events for four aspect ratios and demonstrates the second-order polynomial trend of the elongation ratios ( $\tilde{T}_s/T_s$ ) vs. ( $r_k$ ). The flexible-base modal frequency corresponds to the peak amplitude of the transmissibility function defined in Section 6.1, which was computed using the acceleration recordings of the roof/free field pair. The free field and structure's top motion are the input and output signals of the flexible-base system. As shown, ( $\tilde{T}_s/T_s$ ) increases with the stiffness ratio for all values of the aspect ratio,

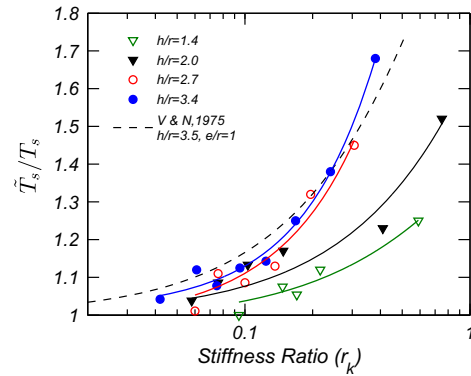


**Fig. 9.** Variation of period elongation ratio with the stiffness and aspect ratio.

noting that the structure with high stiffness and aspect ratios can undergo large elongation ratio. This implies a significant influence of ( $r_k$ ) and the aspect ratio ( $A$ ) on the inertial interaction effects, and the inertial interaction might be crucial for relatively rigid tall and slender structures. This is consistent with the findings of Stewart et al. [38] from field test data in which stiff structures with higher stiffness ratios and natural fixed-base periods ( $T_s$ ) of less than 1.0 s have experienced period elongation. However, no significant period elongation has been observed for structures with natural periods greater than 1.0 s.

Also, Fig. 9 compares the estimated values of ( $\tilde{T}_s/T_s$ ) with the analytical results of Veletsos and Nair [13,39] for the structure with aspect ratios of 3.5. As mentioned, the foundation embedment ratio ( $e/r$ ) was assumed 0.25 in this study, however, as shown in Fig. 9, the trends of elongation ratio estimated using nonlinear FE method are approximately consistent with elongation trend proposed by Veletsos and Nair for  $e/r=1$ . This comparison reveals that current 3-D nonlinear model predicts stiffer foundation than 2-D analytical models. Such a high estimation of dynamic foundation stiffness can be attributed to the dynamic interaction of soil and foundation wall, 3-D dynamic stiffness, i.e. cross-coupling and rotational stiffness that are accounted for by current FE model.

Focusing on the trend of the curves (Fig. 9), a few irregularities with the data orders are observed. Firstly, for the  $h/r=2.0$  with lower stiffness ratio, a higher elongation ratio is shown compared to the other curves. The modal period of the soil deposit and the predominant frequency of the input motion (Northridge) seem to coincide with the natural period of the structure ( $T_s = 0.6$  s), causing the system to resonate.

##### 6.4.2. Rocking motion of system

It has been well understood that rocking motion of foundations partially or fully embedded in soil medium plays a major role in inertial SSI [35], and can further clarify coupled structure-foundation motion in conjunction with translational motion and period elongation of flexible-base structure. In this study, since each node of soil and foundation has three degree of freedom, the vertical differential motions of nodes on opposite sides of foundation were used to obtain rocking motion of foundation. The representative results for foundation rocking motion of relatively tall (thickened outlines) and short (thin outlines) structures with low and high stiffness ratios are presented in Fig. 10. It is worth noting that tall and short structures with the respective fixed-base periods of  $T_s = 0.5$  s and  $T_s = 0.2$  s are extreme cases that might rarely happen, and their rocking motion are depicted in Fig. 10 just to confirm the role of high stiffness ratio. Two zones of peak rocking response can be observed in this figure where in the zone labeled as “natural foundation rocking” ( $T \approx 0.2-0.3$  s), rocking motion is mainly

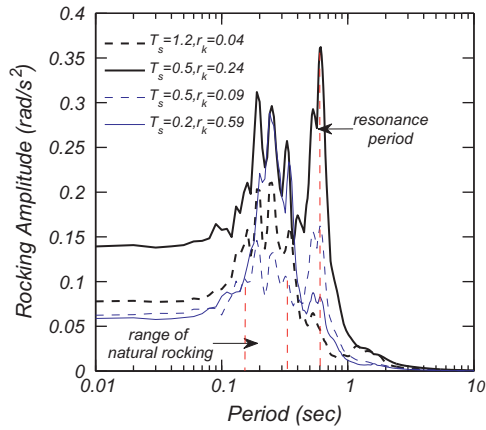


**Fig. 10.** Rocking motion of system for structures with  $h/r = 3.4$  (thickened outlines) and  $h/r = 1.4$  (thin outlines).

influenced by combined relative stiffness and aspect ratios. As shown, for example, stiff tall structure ( $T_s = 0.5$  s,  $r_k = 0.24$ ) exhibits largest rocking spectra among other structures over entire period range while flexible short structure ( $T_s = 0.5$  s,  $r_k = 0.09$ ) experiences lowest level of rocking amplitude. The spectral rocking amplitude of stiff short structure ( $T_s = 0.2$  s,  $r_k = 0.59$ ) is larger than that of flexible tall one over a broad range of period ( $0.2 < T < 1.0$  s), further emphasizing the role of stiffness ratio. In the other zone labeled as “resonance period ( $T = 0.6$  s.)”, the resonance happens between soil, structure and input motions since flexible-base period of system coincides the second fundamental period of soil deposit ( $T = 0.6$  s, shown in Fig. 7) and predominant period of input motion at the bedrock level ( $f_p = 1.67$  Hz for Northridge motion, shown in Fig. 6). Such a case which is named as “double resonance” by Mylonakis et al. [35] leads to significant increase of system response shown for both tall and short structures with fixed-base period of 0.5 s.

6.4.3. Effect of SFSI on FIM

The foundation-structure system subjected to a ground motion is a coupled system [12] in which the responses of both components affect each other. Fig. 11a and b plots the deviation of the foundation motion ( $u_f(\omega)$ ) from the free field ( $u_g(\omega)$ ) due to structural inertial force in a normalized frequency domain with respect to the flexible-base natural period of structure ( $\tilde{T}_s$ ) for two aspect ratio values ( $h/r = 1.4$ ,  $h/r = 3.4$ ). The amplitude of the deviation of motion is expressed using the transfer function (Section 6.1) calculated from the cross and auto power spectra of the foundation and free field displacement motions. These plots clarify how the vibration of structure with various relative stiffness and aspect ratios can influence foundation motion relative to the free field. As shown, the foundation motion of tall structures ( $h/r = 3.4$ ) is amplified at  $T/\tilde{T}_s \approx 1$ , demonstrating that the structure and foundation resonate at flexible-base period of the structure. Also, the amplification of foundation motion is pronounced as the structure becomes stiffer relative to the foundation such that the foundation motion of structure with  $r_k = 0.24$  is amplified 50% ( $u_f(\omega)/u_g(\omega) = 1.5$ ). Moreover, comparing transfer functions of tall structures with various relative stiffness (Fig. 11b) reveals the role of relative stiffness ratio in deviation of foundation motion from free field motion as transfer function corresponding to the structure model with  $r_k = 0.04$  exhibits much less amplification. In other words, there is low SSI effect acting in the system, and foundation of such a flexible tall structure follows the free field motion, causing the structure to vibrate similar to the fixed-base condition. On the other hand, the peaks of transfer functions corresponding to

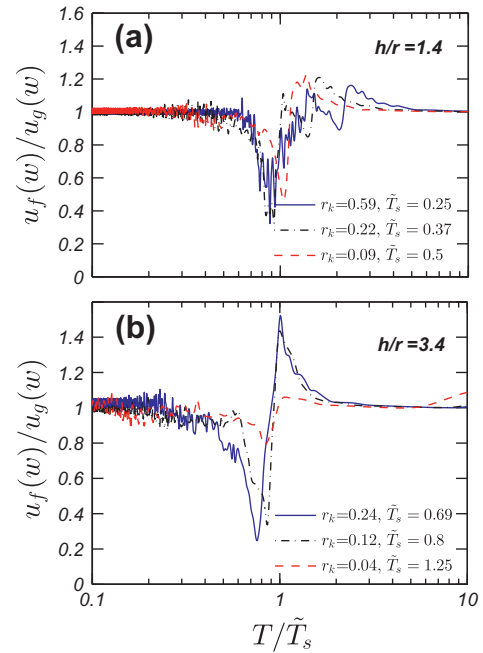


**Fig. 11.** Foundation/free field transfer function under inertial interaction in normalized frequency domain for various stiffness ratios (a)  $h/r = 1.4$  and (b)  $h/r = 3.4$ .

short structures occur at period ratio of  $T/\tilde{T}_s > 1$  with level of amplification  $u_f(\omega)/u_g(\omega)$  up to 1.22 depending on the stiffness ratio ( $r_k$ ) as shown in Fig. 11a. Such deviation from flexible-base period of structure along with low amplification level implies lower impact of short structure on vibration of foundation.

Fig. 11a and b also depicts de-amplification with maximum amplitude occurring at or close to the period ratio of  $T/\tilde{T}_s = 1$ . The amplitude of de-amplification seems to be affected by variation of stiffness ratio for tall structures such that foundation of the tall structure with  $r_k = 0.04$  undergoes slight de-amplification (Fig. 11b) while foundation of the short structure exhibits much less sensitivity to variation of the stiffness ratio (Fig. 11a).

The comparison between foundation responses of short and tall structures indicates that the aspect ratio has significant contribution to the coupled structure-foundation oscillation. Accordingly, rigid tall structure ( $r_k = 0.24$ ,  $h/r = 3.4$ ) can highly influence foundation motion both in terms of vibration frequency and amplitude (amplification or de-amplification) while foundation of short structure shows insensitive response to the relative foundation-structure stiffness. The high influence of structure on foundation motion by tall structure can be explained by imposed rocking motion as shown in Fig. 10.

6.4.4. Effect of SFSI on base shear demand

To evaluate the effect of SFSI on base shear demand, the fixed-base analyses were also performed, and their results were compared with those of flexible-base analyses. Base shear is defined as the product of the mass and acceleration of the structure’s top. In fixed-base analysis, the free field ground motion is used as the foundation input motion whereas the foundation is restricted against any translational and rotational motion or the rigidity of the supporting soil becomes infinity ( $\sigma \rightarrow \infty$ ). The acceleration response spectra plots of each structure’s top, which mainly produces base shear, are shown in Fig. 12 for fixed and flexible-base motions of stiff 4-story (Fig. 12a) and 10-story (Fig. 12b) buildings with stiffness ratios of  $r_k = 0.59$  and  $r_k = 0.38$ , respectively. Stiff structures were selected because of the strong influence

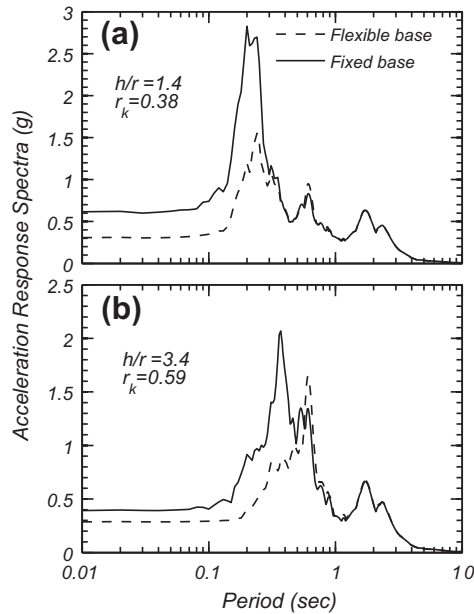


Fig. 12. Fixed base vs. flexible base response spectra of structure's top (base shear demand) for structures with (a)  $h/r = 1.4$ ,  $r_k = 0.38$  and (b)  $h/r = 3.4$ ,  $r_k = 0.59$ .

of the inertial interaction on them as discussed in Sections 6.4.1–6.4.3. These plots demonstrate the alteration of the modal damping and period due to SSI. This has both beneficial and detrimental impacts on the response of linear structures. As shown, significant attenuation in the spectra occurs in both cases up to the flexible-base natural period of the structure. After this point, in the case of a 10-story building, the rocking motion in the flexible-base gives rise to spectra that exceed the values for the fixed-base scenario as shown in Fig. 10. No major amplification is observed in the 4-story case. This reduction in base shear demand is a consequence of the energy dissipation by the flexible-base damping ( $\zeta$ ), which includes both the frequency dependent soil–foundation radiation damping and the hysteretic damping of the soil. Such a reduction in base shear demand, and alteration in the modal properties due to SSI, implies a beneficial effect of SSI over a range of periods. This effect has been proposed by NEHRP 1997 [33,40]. However, similar to the rigid 10-story building case herein, there are some case histories in which SSI has been detrimental. Shifting of the natural period of tall rigid structures to the long period range, where amplification of earthquake motion subsequently occurred due to geological site conditions, has resulted in damage to the structure. This detrimental aspect of SSI has not been predicted by seismic

building codes which propose design spectral amplitudes decreasing monotonically after a period of 1.0 s [40].

### 6.5. Effect of input motion on inertial interaction

As mentioned, the Loma Prieta 1989 and Northridge 1994 earthquakes were employed to investigate the effect of the input motion on SFSI. Three models with various aspect ratios and periods were subjected to these input motions. Fig. 13 plots the influence of the frequency content and intensity level of the input motion on the inertial interaction. The results are expressed by the transfer function between the free field and the top of the structure's motion in normalized frequency domain with respect to the fixed-base period of the structure ( $T_s$ ). The period ratio ( $T/T_s$ ) corresponding to the peak of transfer functions demonstrates period elongation ratio due to inertial interaction, and the amplitudes show level of amplification of free field motion at natural period of system. As shown, both input motions cause almost the same period elongation ratio in all cases, however, for the case of a structure with  $T_s = 0.6$  s (Fig. 13b), both transfer functions exhibit the same amplitude. The second mode fundamental period of soil deposit is shown to be 0.6 s (second peak) (Fig. 7b). Therefore, it seems that natural period of the structure coincides with the second mode period of the soil deposit, resulting in soil–structure system resonance. This case is also confirmed in Section 6.4.3 by Fig. 11. For the other two cases (Fig. 13a and c), the structures subjected to the Loma Prieta earthquake experience higher foundation damping (lower amplification). This could be due to higher soil material damping generated by Loma Prieta motion due to its higher PGA than Northridge motion.

## 7. Conclusions

This paper investigates effects of site response and dynamic soil–structure interaction on performance of linear elastic structures supported by inelastic soft soil. For this purpose, a three dimensional Finite Element model utilizing kinematic hardening elasto-plastic soil model and linear SDOF structure were employed. The numerical model that was developed in the framework of OpenSees was shown to be fully capable of simulating seismic site response and soil structure interactions, as validated by comparisons with centrifuge test results. Using the Loma Prieta and Northridge earthquakes as real-world input data, this numerical modeling program was used to investigate various aspects of SSI effects and clarify dynamic performance of soil–structure system. Several conclusions were drawn from this parametric study:

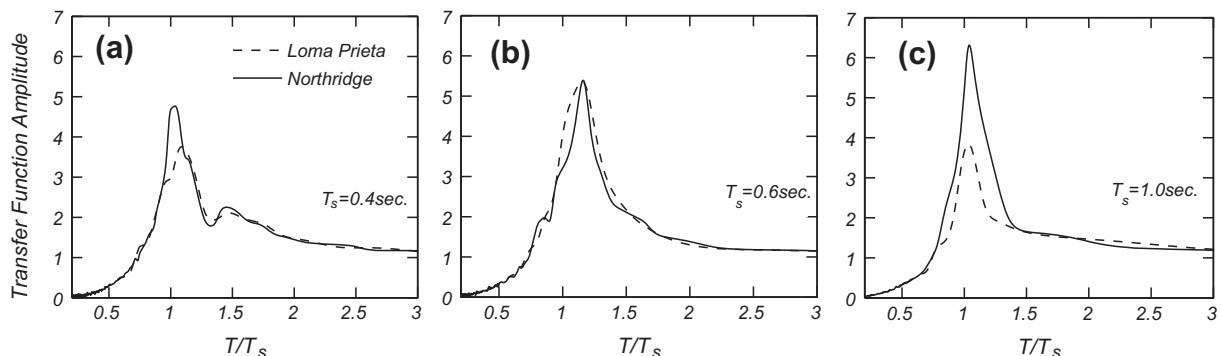


Fig. 13. Effect of input motion on inertial interaction of structures with (a)  $T_s = 0.4$  s (b)  $T_s = 0.6$  s, and (c)  $T_s = 1.0$  s.

1. The kinematic interaction was shown to reduce foundation input motion over effective frequency range of the soil–structure system as subjected to the free field ground motion. The foundation/free field transfer function demonstrated frequency dependent trend which reveals the role of radiation damping in deviation of foundation vibration. Comparison between results of this study with those of analytically derived with visco-elastic soil assumption, reveals that soil plasticity can affect radiation damping of the foundation.
2. It was shown that aspect ratio and structure–foundation relative stiffness ratios are crucial parameters characterizing various aspects of inertial soil–structure interaction. The combined large values of these two parameters may cause structure vulnerable to the inertial soil–structure interaction. This implies that rigid tall structures can undergo significant natural period elongation along with considerable foundation rocking which was mainly found to be controlled by the aspect ratio.
3. The rocking motion of system which is dominant in tall structures may cause coupled system of foundation–structure to oscillate at the flexible–base frequency of structure. Depending on relative stiffness ratio of structure, foundation motion exhibits either significant deviation or complies with free field motion.
4. The potential resonance between components involved in SSI phenomenon must be taken into account in any seismic analysis. This hazardous event is of great significance in thick deposit of soils with low shear wave velocities, in which modal fundamental periods of site are likely to coincide the natural periods of structure. For tall structures, it was concluded that resonance can occur between structure, input excitation and soil deposit.

In conclusion, the results of this study indicate the significance of seismic performance-based design in short to mid-rise structures resting on shallow foundation and elasto-plastic soft soil. It was also shown that detailed characterization of soil–structure interaction is crucial for this type of site–structure setting to avoid hazardous events like resonance, foundation rocking and excessive base shear demand.

### Acknowledgement

This research was funded by Natural Sciences and Engineering Research Council of Canada (NSERC). The authors would like to thank NSERC for this financial support.

### References

- [1] Seed RB, Dickenson SE, Mok CM. Recent lessons regarding seismic response analyses of soft and deep clay sites. In: Proceedings of seminar on seismic design and retrofit of bridges. Earthquake Engineering Research Center, Univ. of California at Berkeley, California Dep. of Transportation, Sacramento, Calif., 1992, p. 18–39.
- [2] Veletsos AS, Prasad AM, Wu WH. Transfer functions for rigid rectangular foundations. *Earthquake Eng Struct Dynam* 1997;26(1):5–17.
- [3] Luco JE, Wong HL. Response of a rigid foundation to a spatially random ground motion. *Earthquake Eng Struct Dynam* 1986;14:891–908.
- [4] Bielak J. Dynamic behavior of structures with embedded foundations. *Earthquake Eng Struct Dynam* 1975;3(3):259–74.
- [5] Veletsos AS, Meek JW. Dynamic behavior of building–foundation systems. *Earthquake Eng Struct Dynam* 1974;3(2):121–38.
- [6] Veletsos AS, Verbic B. Vibration of viscoelastic foundations. *Earthquake Eng Struct Dynam* 1973;2(1):87–102.
- [7] Mita A, Luco JE. Dynamic response of square foundation embedded in an elastic half-space. *Soil Dynam Earthquake Eng* 1989;8(2):54–67.
- [8] Gazetas G. Formulas and charts for impedances of surface and embedded foundations. *J Geotechn Eng (ASCE)* 1991;117(9):1363–81.
- [9] De Barros CP, Luco JE. Identification of foundation impedance functions and soil properties from vibration tests of the Hualien containment model. *Soil Dynam Earthquake Eng* 1995;14(4):229–48.
- [10] Tileyliglu S, Stewart JP, Nigbor RL. Dynamic stiffness and damping of a shallow foundation from forced vibration of a field test structure. *J Geotechn Geoenviron Eng (ASCE)* 2011;137(4):344–53.
- [11] Kim S, Stewart JP. Kinematic soil–structure interaction from strong ground recordings. *J Geotechn Geoenviron Eng* 2003;129(4):323–35.
- [12] Safak E. Detection and identification of soil–structure interaction in buildings from vibration recordings. *J Struct Eng (ASCE)* 1995;121(5):899–906.
- [13] Stewart JP, Fenves GL, Seed RB. Seismic soil–structure interaction in buildings I: analytical methods. *J Geotechn Geoenviron Eng (ASCE)* 1999;125(1):26–37.
- [14] Kim YS, Roesset JM. Effect of nonlinear soil behavior on inelastic seismic response of a structure. *J Geotechn Geoenviron Eng (ASCE)* 2004;4(2):104–14.
- [15] Rayhani MHT, Elnaggar MH. Numerical modeling of seismic response of rigid foundation on soft soil. *Int J Geomech (ASCE)* 2008;8(6):336–46.
- [16] Rayhani MT, El Naggar MH. Centrifuge modeling of seismic response of layered soft clay. *Bull Earthq Eng* 2007;5(4):571–89.
- [17] Stewart JP, Seed RB, Fenves GL. Empirical evaluation of inertial soil–structure interaction effects. Report No. PEER-98/07 1998, Pacific Earthquake Engineering Research Center, Univ. of California, Berkeley, Calif.
- [18] Zhang J, Tang Y. Dimensional analysis of structures with translating and rocking foundations under near-fault ground motions. *Soil Dynam Earthquake Eng* 2009;29:1330–46.
- [19] Mazzoni S, McKenna F, Fenves GL. Open system for earthquake engineering simulation user manual. Berkeley: Pacific Earthquake Engineering Research Center, University of California; 2010. <<http://OpenSees.berkeley.edu/>>.
- [20] Prevost JH. Mathematical modelling of monotonic and cyclic undrained clay behaviour. *Int J Numer Anal Methods Geomech* 1977;1(2):195–216.
- [21] Elgamal A, Yang Z, Parra E, Ragheb A. Modeling of cyclic mobility in saturated cohesionless soils. *Int J Plast* 2003;19:883–905.
- [22] Gu Q, Conte JP, Yang Z, Elgamal A. Consistent tangent moduli for multi-yield-surface J2 plasticity model. *J Comput Mech* 2011;48(1):97–120.
- [23] Wolf JP. Dynamic soil–structure interaction. Englewood-Cliffs, New Jersey: Prentice-Hall; 1985.
- [24] Boulanger RW, Curras CJ, Kutter BL, Wilson DW, Abghari A. Seismic soil–pile–structure interaction experiments and analyses. *J Geotechn Geoenviron Eng (ASCE)* 1999;125(9):750–9.
- [25] Elgamal A, Yang Z, Lai T, Kutter B, Wilson D. Dynamic response of saturated dense sand in laminated centrifuge container. *J Geotechn Geoenviron Eng (ASCE)* 2005;131(5):598–609.
- [26] Rayhani MHT, El Naggar MH. Characterization of glyben for seismic application. *Geotechn Test J (ASTM)* 2008;31(1):24–31.
- [27] Turan A, Hinchberger SD, Elnaggar MH. Mechanical characterization of an artificial clay. *J Geotechn Geoenviron Eng (ASCE)* 2009;131(2):280–90.
- [28] Jeremic B, Kunnath S, Xiong F. Influence of soil–foundation–structure interaction on seismic response of the I-880 the viaduct. *Int J Eng Struct* 2004;26(3):391–402.
- [29] Chopra AK. Dynamics of structures: theory and applications to earthquake engineering. 3rd ed. Upper Saddle River, New Jersey: Pearson Education Inc.; 2007.
- [30] Diaz ND, Amat PS. GiD the personal pre/postprocessor user's manual, version 5.0, CIMNE, Barcelona, Spain; 1999. <<http://gid.cimne.upc.es>>.
- [31] Pandit SM. Modal and spectrum analysis. New York: John Wiley; 1991.
- [32] Seed HB, Romo MP, Sun JI, Lysmer J. The Mexico earthquake of September 19, 1985–relationships between soil conditions and earthquake ground motions. *Earthquake Spectra (EERI)* 1988;4(4):687–729.
- [33] Kramer SL. Geotechnical earthquake engineering. New Jersey: Prentice Hall Inc.; 1996.
- [34] Elsabee F, Morray JP. Dynamic behavior of embedded foundation. Rep. No. R77–33, Dept. of Civil Engineering. Massachusetts Institute of Technology, Cambridge, Mass; 1977.
- [35] Mylonakis G, Nikolaou S, Gazetas G. Footings under seismic loading: analysis and design issues with emphasis on bridge foundations. *Soil Dynam Earthquake Eng* 2006;26:824–56.
- [36] Zhang J, Tang Y. Radiation damping of shallow foundations on nonlinear soil medium. In: Proceedings of fourth international conference on earthquake geotechnical engineering. Thessaloniki, Greece; 2007.
- [37] Aviles J, Perez-Rocha JE. Site effects and soil–structure interaction in the valley of Mexico. *Soil Dynam Earthquake Eng* 1998;17(1):29–39.
- [38] Stewart JP, Seed RB, Fenves GL. Seismic soil–structure interaction in buildings II: Empirical findings. *J Geotechn Geoenviron Eng (ASCE)* 1999;125(1):38–48.
- [39] Veletsos AS, Nair VV. Seismic interaction of structures on hysteretic foundations. *J Struct Eng (ASCE)* 1975;101(1):109–29.
- [40] Mylonakis G, Gazetas G. Seismic soil–structure interaction: beneficial or detrimental? *J Earthquake Eng* 2000;4(3):277–301.